

Molecular Line Emission in the ISM

Radio and (more recently) sub-millimeter observations of line emission from molecules is one of the most useful ways to study the ISM. Many molecular species have been detected in the dense clouds that are found at random in the disk. These aptly named molecular clouds contain the bulk of the mass of the ISM, although their volume fraction is relatively small. Here I will discuss some of the background physics of molecular line emission and present various observational results.

Section 1: Units in Radio Astronomy

When radio astronomy first developed people were observing continuum sources such as HII regions. For such objects the temperature of the emission region—so far as such can be defined, bearing in mind that the gas is not in thermodynamic equilibrium—is of order 10^4 K and so for radio frequencies we have that $h\nu \ll kT$. In such a case the blackbody formula reduces to the Rayleigh-Jeans approximation

$$B_\nu(T) = \frac{2k\nu^2}{c^2} T \quad (3.1)$$

so at a given frequency the blackbody specific intensity is strictly proportional to T . If one assumes that this is generally true then one can write

$$T = \frac{c^2}{2k\nu^2} I_\nu . \quad (3.2)$$

Recalling that I_ν is the same as surface brightness on the sky then for a uniform sky brightness over an angular region of solid angle Ω one has that $I_\nu = P_\nu/\Omega$ where P_ν is the total flux density observed within the region. Thus if these two results are put together one can write

$$T = \frac{c^2}{2k\nu^2\Omega} P_\nu \quad (3.3)$$

which relates the flux density received looking at some sky area to the temperature.

When observing with a radio telescope one normally detects some fraction of the incident energy—perhaps 50 to 70%. The telescope is sensitive to some region on the sky around the direction it is pointed (and backwards, which occasionally causes problems!) as well as to signals from other directions. This leads to various practical problems in carrying out radio observations. None the less, most of the telescope sensitivity is on some area of the sky around the pointing direction, in what is called the *main beam*. Sensitivity to sources in other directions is due to *side-lobes*.

The beam is usually described by approximating it as a circular gaussian function of angle away from the direction of pointing. The angular size of the main beam defines a Ω value for the telescope. The if one knows the efficiency of the main beam, denoted as η , and one is observing a uniform region of sky then the flux density detected is

$$p_\nu \approx \eta\Omega I_\nu \approx \eta\Omega \frac{2k\nu^2}{c^2} T . \quad (3.4)$$

What is actually measured is the power collected by the telescope over a frequency range, something like $P = p_\nu A \Delta\nu$ where A is the telescope surface area. The result is still directly proportional to T if the Rayleigh-Jeans approximation holds and if a uniform area of sky is observed.

Of course the sky emission will not be uniform, and the Rayleigh-Jeans approximation may not hold for the sources in the field of observation. Still, one can define the *brightness temperature* directly from a measured P value if the various constants required are known. So once the telescope beam size is measured, and the η value is measured as best as is possible, for given $\Delta\nu$ and ν each T value corresponds to a given sky brightness and hence to an I_ν value for the field of view. Thus radio measurements are often reported directly in terms of T_A , the *antenna temperature*. The formal definition of T_A is that it is the temperature for which the telescope would observe the same total power assuming that the blackbody filled the whole field of view of the telescope, main beam and side-lobes; also it is assumed that the Rayleigh-Jeans approximation to the blackbody function holds for all levels of emission. Of course once T is of the same order as $h\nu/k$ the Rayleigh-Jeans approximation breaks down. In such a case the T value from the Rayleigh-Jeans approximation will be much smaller than the actual temperature of the source. Also the “real” temperature of the emission will be T_A/η since the telescope does not detect all the radio energy incident on it.

To make an analogy with optical astronomy, reporting the T_A value for a given position is like using a photometer to find the total power received in a given filter, say the V filter, when looking at a given direction but then expressing the result as sky brightness in magnitudes per square arc-second or some other such units from the telescope field of view. In doing this one does not know whether the emission is from one star in the field or from a nebula or from several stars together. Now if a single star is in the field of view it will be very tiny in angular size compared to the telescope field of view, but that is not the number that will be reported since things are given on a per solid angle of sky basis.

This leads to the concept of beam dilution. What is observed is the total flux density

in the telescope field, which is given by

$$F_\nu = \int_{\Omega} I_\nu d\Omega \quad (3.5)$$

which is set to $\Omega \bar{I}_\nu$. Then the \bar{I}_ν is used to calculate the T_A value. Then clearly

$$\bar{I}_\nu = \frac{\int I_\nu d\Omega}{\Omega} \quad (3.6)$$

but there are many ways to get the same \bar{I}_ν for a given Ω value. (The above equation should really be weighted by a relative telescope efficiency as a function of sky position, but this does not change the line of reasoning.) For example assume that I_ν is zero over most of the field and constant within a small solid angle α . In that case

$$\bar{I}_\nu = \frac{\alpha}{\Omega} I_\nu \quad (3.7)$$

and thus if both I_ν values are expressed as temperatures one has

$$T_B = \bar{T} = \frac{\alpha}{\Omega} T . \quad (3.8)$$

Thus if the radio telescope beam is larger than the source, the temperature which is derived is systematically too small due to the beam size. This is more of an issue for single-disk radio telescopes or sub-millimeter telescopes where the field of view is large, and less of an issue for radio interferometry observations where the angular resolution can be very good...but when interferometry is done the resulting images usually do not give an accurate global brightness.

Section 2: Hydrogen 21 cm Emission

As seen earlier in these notes, in the far-infrared the only atomic lines that are observed are due to fine structure transitions in the ground state. For a line to have a wavelength of 300 μm the photon energy is 0.00413 eV and the corresponding frequency is 10^{12} Hz or 1000 GHz. So the photon energies of radio waves are of order a few times 10^{-5} to 10^{-6} eV, far smaller than the typical level separations in atoms. The hydrogen $n = 101$ to $n = 100$ transition has a frequency of 6.48 GHz so there can be normal transitions at such frequencies, but exciting hydrogen to the $n = 101$ state requires a high temperature. At low temperatures with the atoms mostly in the ground state such transitions are not available.

There are few fine structure or hyperfine transitions at very low frequencies. For hydrogen the only available ground state transition is a hyperfine transition caused by an interaction between the electron spin and the proton spin. This transition is between the $F = 0$ ground state and the $F = 1$ upper state, the latter of which has statistical weight 3. Thus the lowest energy state is one with the spins opposed. The spin-flip transition is forbidden by the $\Delta F = 0$ selection rule, and both states have no electric dipole moment. Thus the transitions have to occur via the electric quadrupole mode, and the transition rates are very small. The transition occurs at a frequency of 1.4204 GHz.

Weak as the transition is, it is the only tracer of cold hydrogen atoms in the ISM. It turns out the emission is marginally optically thick in the disk of the Galaxy. Maps have been made of the emission, although generally at low resolution compared with the CO line surveys to be discussed later. The 21 cm emission shows systematic doppler shifts with direction which are due to Galactic rotation.

It is found that the HI gas is mostly absent in the inner 3 kpc or so of the disk, aside from an inner tilted ring which will be described later. The surface density of HI (that is, the integrated column density in the direction perpendicular to the galactic plane) stays more or less constant out to beyond the solar circle to 14 kpc, and then declines. It can be traced out to at least 25 kpc, farther than any other tracer of the disk. Since the area of the disk is increasing as r^2 , this means that the majority of the mass of HI in the Galaxy is beyond the solar circle; perhaps more than 70%. It is clear from the kinematics of the gas near the Galactic center direction that what HI there is in the innermost 3 kpc is subject to significant non-rotational motions, which messes up the determination of the mass function at these small radii. The HI gas beyond the solar circle, or beyond the main stellar disk in external galaxies, is the source of the most direct evidence of dark matter in spiral galaxies, since it usually implies a flat rotation curve out to large radii. Indeed, in lower mass galaxies the rotation curve seems to often rise at large radii. There is fairly good correlation between the dark matter mass and the total HI mass, which may indicate that the dark matter is made up of diffuse cold molecular gas rather than exotic particles.

It appears that the HI gas layer ends only when the intergalactic diffuse UV radiation ionizes the atoms. We also know that the HI disk is warped at large radii, a behavior that is typical of disk galaxies. The cause for the warp is still not known.

In addition to the main HI layer with thickness ± 220 pc inside the solar circle, there is a lower density extended layer called the Lockman layer which is roughly twice as thick. Outside the solar circle both components flare out.

Section 2-1: High-Velocity Clouds

In the 1960's when HI line maps were first being made it was found that there are various clouds at high galactic latitudes, which have radial velocities which do not match the Galactic rotation curve. These *high-velocity clouds* have been a puzzle for ISM researchers for a long time. The first discovered HVC, now named HVC-Chain A, is a 30° long filament of gas which is well off the galactic plane in the second quadrant. The various knots of bright CO emission in this cloud have radial velocities between -210 and -140 km/s relative to the local standard of rest. This motion cannot be due to normal rotation in the disk of the galaxy.

The nature of these HVCs is still not firmly established. Some of them appear to be small local clouds that are not too far off the plane of the disk. However many of them have fairly large lower limit distances and it is not clear where they are in the Galaxy. Indeed, the HVCs may not be part of the Galaxy at all but may rather be gas clouds in the local group in some cases.

Recently HST measurements of line absorptions from this particular HVC have established some limits on its distance. It is more than about 4 kpc away because the spectrum of a star, PG0859+593, at that distance does not show any HI absorption from the HVC-Chain A cloud. Then observations of the halo RR Lyrae star AD UMa, for which a distance of 10 kpc is derived from the period-luminosity relation, have shown that the absorption from HVC-Chain A is present in the optical spectrum near the Ca^+ H and K lines. So the cloud is between 4 and 10 kpc away, and thus is between 2.5 and 6.3 kpc off the galactic plane.

Figure 19 shows a map of the HVCs superimposed on the old Lund optical picture of the Galaxy. Cloud HVC-Chain A is marked to the left of center and above the plane. The very prominent elongated gas cloud in the south is the magellanic stream, connecting the SMC and the LMC with a trailed wake of gas going to the south galactic pole. It is thought to mark the orbit of the Magellanic clouds, and to be the result of tidal forces from the Galaxy.

The radial velocity of AD UMa is $+77$ km/s, which is what is expected for a halo object in that direction and at 10 kpc distance. The cloud absorption lines seen in its spectrum are at -160 km/s. If the cloud is halfway in between the two limits then its random velocity with respect to the local rotation speed is about -130 km/s.

For this cloud given the distance estimate the mass can be found. While it is not well constrained, it is in the range $2 \cdot 10^5$ to $2 \cdot 10^6 M_\odot$. The absorption line studies imply that this cloud has a low metallicity and may be an intergalactic hydrogen cloud which has been captured by the Milky Way galaxy. Given the mass and velocity estimates, the cloud has a very large kinetic energy, of order 10^{46} J. This is far larger than the energy of a

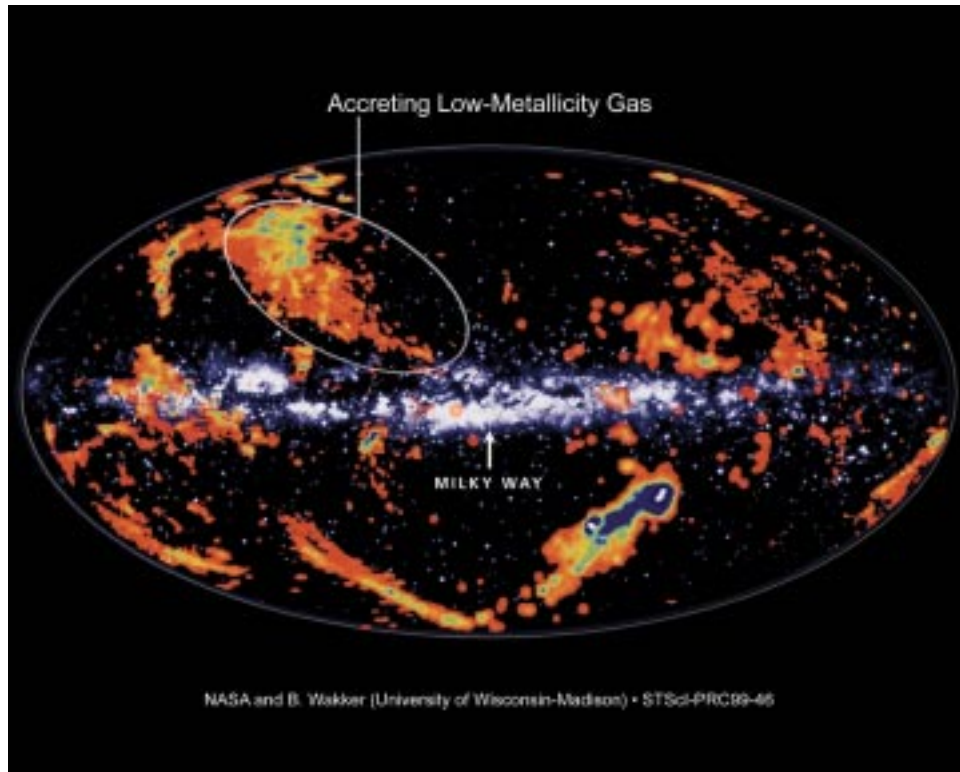


Figure 19—A map of the HI clouds superimposed on the Lund optical picture of the Milky Way. The HI map is from the Dwingeloo 21 cm survey, and is colour coded in total intensity such that blue shows the most intense emission and red shows the least intense emission. This image is courtesy of B. P. Walker.

supernova explosion.

One nice thing about this picture is that it explains, at least in part, how the Galaxy can continue to form stars over its entire existence without running out of gas. If clouds are still raining down onto the disk at intervals, it will replenish the gas mass in the disk.

Section 3: Molecular Emission

While atoms do not produce many lines at infrared or radio wavelengths, molecules produce many such lines. These are possible due to vibrational and rotational transitions, which only occur with two or more nuclei. The energies of such transitions cover a very wide range, but a general rule of thumb is that molecular vibrational transitions occur at mid-infrared to optical or even UV wavelengths, while rotational transitions are rather less energetic and occur at far-infrared to radio wavelengths. The optical spectra of cool stars show a number of molecular bands of small molecules such as TiO, for example, but I am not aware of any pure rotational lines at optical wavelengths.

Under cold conditions in the ISM it is the rotational transitions and some atomic fine-structure transitions which carry most of the radiation from the gas. Historically the first rotational transitions which were detected were from maser lines, which occur in star formation regions and in the circumstellar envelopes of late-type stars. These will therefore not be discussed here. Since the vibrational lines are not as often observed from the general ISM, I will concentrate on rotational spectra.

Section 3–1: Rotational Lines

All molecules have moments of inertia and an energy of rotation. As the energy levels are quantized, this leads to rotational transitions which can be observed. In classical mechanics any extended object has three principle moments of inertia, which simplify the inertia tensor to diagonal form and produce simple expressions for the rotational energy and the angular momentum. This carries over to quantum physics, and so it is customary to classify the rotational characteristics of molecules based on the values of the principle moments of inertia. Calling these I_a , I_b , and I_c in order of increasing magnitude, a molecule which is linear or has an axis of rotational symmetry is called a *symmetric top* type molecule. Then either $I_c = I_b > I_a$ or $I_c > I_b = I_a$. Linear molecules will have a small I values about the axis of the molecule so they are of the first variety, the *prolate symmetric rotor* case. Other molecules, such as benzene for example, have the largest moment of inertia about the symmetry axis and are called *oblate symmetric rotors*. Molecules which are spherically symmetric, such as C_{60} or CH_4 have three equal moments of inertia and are called *spherical rotors*, while various more complicated molecules have three distinct moments of inertia and are called *asymmetric rotors*.

The angular momentum of the rotating molecule is quantized with magnitude and z component

$$|\vec{P}_J| = \sqrt{J(J+1)} \hbar \quad P_{Jz} = J\hbar \quad (3.9)$$

using J for the rotational quantum number which has integer values from 0 up. If the moment of inertia of the rotation is constant, then the energy, $P^2/2I$, has the simple form

$$E = \frac{J(J+1)\hbar^2}{2I} = \frac{1}{2}I\omega^2. \quad (3.10)$$

For real molecules I depends on J to some degree, but often the rigid rotator assumption is an excellent approximation. The quantum mechanical requirements for electric dipole transitions are that (a) the molecular dipole moment $\vec{\mu}$ is non-zero, (b) $\Delta J = \pm 1$, and (c) $\Delta M_J = 0, \pm 1$, where M_J is the quantum number for the z component of the angular momentum. This last condition is of no importance unless the molecules are in an electric

or magnetic field. Rotational level J has statistical weight $2J + 1$. This type of expression applies to symmetric rotator molecules. Things turn out to be much more complicated for asymmetric rotor molecules.

The condition on the dipole moment $\vec{\mu}$ means that some molecules have no dipole rotational transitions, including diatomic molecules with identical isotopes of the two atoms, such as the most common forms of H_2 , O_2 , and N_2 . This can also eliminate rotational transitions of more complicated molecules such as C_2H_2 in the dominant isotopic form. Where the dipole moment is non-zero the strength of the transition is proportional to its magnitude μ . The value of μ is conventionally expressed in Debye units, 1D being equal to $3.33564 \cdot 10^{-30}$ Cm. HD has a very small μ value of 0.00059 D, whereas CO has μ of 0.112 D and SO has μ of 1.55 D.

With the energy equation above and ΔJ of 1 the transitions have predicted frequencies

$$\nu_J = \frac{h}{4\pi^2 I} J \quad (3.11)$$

where J is the quantum number of the upper state so it will be 1, 2, 3, ... In this approximation, the line frequencies are linear in J . It is customary to write the energy values as

$$E_J = hBJ(J + 1) \quad (3.12)$$

so that $\nu_J = 2BJ$. A similar expression is used with wavenumbers, ν/c , in infrared spectroscopy. Molecules with larger moments of inertia will therefore have lower frequencies for their rotational transitions. For real molecules where the energy deviates from the expression above people normally use fitting functions of the form

$$E_J = h [BJ(J + 1) - DJ^2(J + 1)^2 + HJ^3(J + 1)^3 - \dots] \quad (3.13)$$

to describe the energy level structure and the line frequencies of symmetric rotor molecules. This type of description applies to all diatomic molecules and a number of more complex linear chain molecules. Matters become much more complex for other molecular geometries, and more than one quantum number is generally needed to specify the rotational state.

Figure 20 shows the lowest 9 rotational levels of the CO molecule in the ground vibrational state, with the transitions shown. CO is a typical linear molecule and the line frequencies are very close to integer multiples of the $1 \rightarrow 0$ line frequency.

Section 3-2: H_2 Quadrupole Transitions

The only direct observation of molecular H_2 in cooler ISM gas that I have seen in the literature is ISO observations of the quadrupole pure rotation lines of H_2 at 28.2 and

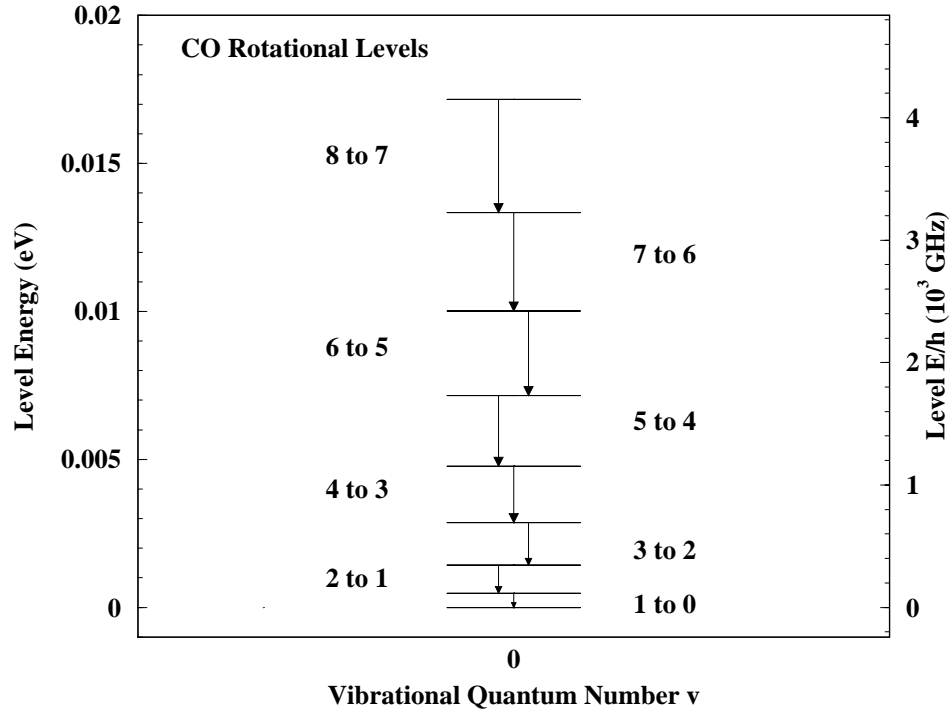


Figure 20—The energy level diagram for the lowest few rotational levels in the CO molecule (with the dominant isotopes of C and of O). The first 8 lines are shown. These have frequencies from 115.271203 GHz up to 921.799706 GHz. Not all of these can be observed from the ground.

17.0 μm . It seems that these lines have been detected previously in absorption, but ISO detected these lines in emission in a few extragalactic star forming regions. These lines were also detected in the NGC 891 galaxy by E. A. Valentijn and P. P. van der Werf (1999; *ApJ*, **522**, L29). What is most interesting about these observations is that the line profiles are interpreted as being due to large amounts of cold H_2 gas, such that the H_2/HI mass ratio is of order 10. The mass so deduced depends upon the temperature assumed for the H_2 gas and its ortho/para ratio. If this result is correct and if it is typical of spiral galaxies, it implies that most of the unseen mass in galaxies is just due to molecular hydrogen rather than due to exotic particles such as massive neutrinos for example.

Section 3–3: Effect of Nuclear and Electron Spin

The nuclear spin has quantum number F . There is interaction between this and the rotational angular momentum, which causes hyperfine splitting of the rotational levels analogous to what occurs in electronic states. Similarly the net electron spin with quantum number S interacts with the rotational angular momentum. These effects depend strongly

on the molecular structure: for molecules such as OH the effects are large, while for CO they are small.

There are some important effects of the nuclear spin on the rotational energy levels for molecules which are symmetric to interchange of some of the nuclei. The most common case is for diatomic molecules where the two nuclei are of the same isotope: depending on the spin of the nuclei, the overall wavefunction has to be symmetric (for bosons) or anti-symmetric (for fermions) to exchange of the nuclei. This adds an additional selection rule for transitions, and the end result is that there are two separate set of energy levels which do not have transitions between them: odd and even J rotational levels are anti-symmetric and symmetric respectively, and if the total wavefunction has to be antisymmetric then odd J rotational levels can only occur if the nuclear spin state is symmetric (spins aligned) while the even J rotational levels can only occur for an antisymmetric nuclear spin state (spins opposed). When the total wavefunction is required to be symmetric then the spin states are switched for given J but the effect is the same.

This then splits the rotational levels into two independent groups, since transitions that change the spin state are forbidden. This also happens in water, where there is symmetry between the two hydrogen atoms. The two forms of the molecule are called *para* and *ortho* forms for the antisymmetric and symmetric nuclear spin states respectively. Since the statistical weights of the two spin states are different, in thermal equilibrium there is a population difference between the para and ortho states. For nuclear spin F the ortho/para ratio is $(F + 1)/F$. Thus for H_2 the ortho/para ratio is 3 since F is $1/2$. If the nuclear spin quantum number is 0 then there is no para form of the molecule, as is the case for O_2 . For diatomic molecules the spin effects make rotational transitions impossible. In more complicated molecules the ortho and para forms are separate but rotational transitions can still occur, because there are several rotational quantum numbers, rather than just one as is the case for diatomic molecules, and thus there is not such a simple division of the symmetry of the states by quantum number as is the case for linear molecules.

Thus for H_2 even if there were a net dipole moment the rotational transitions with $\Delta J = 1$ still cannot occur due to the ortho/para division. The rotational states for each form have J values that differ by 2. Even so the ortho/para division is important for collisional interactions and for vibrational transitions as well.

Section 3–4: Vibrational Bands

In addition to the rotational lines all molecules have vibrational bands corresponding to transitions between various vibrational states. The vibrational quantum number is usually symbolized by v . The energy differences between vibrational states are usually

a few hundred times larger than the spacings between the rotational states. There is no general quantum theory of vibrational transitions, so I cannot present general selection rules for vibrational transitions as I did for rotational transitions.

As the energy difference between vibrational bands is much larger than between the rotational bands (which are present for each vibrational state) any vibrational transition is likely to be accompanied by many rotational transitions which change the energy slightly. Thus when vibrational transitions occur they are almost always in the form of bands of lines with a complex structure. Figure 21 shows the vibrational/rotational levels of the CO molecule, which is a rather simple case. Transitions can occur for $\Delta v = 0, 1, 2, 3, \dots$ and for $\Delta J = 0, \pm 1$. Since there are many closely spaced levels of different J near the lowest level in each vibrational state, the resulting transitions cannot be shown without totally obscuring the level positions. If the vibrations of the molecule resemble those of an harmonic oscillator, which is often the case, then all the combined rotational/vibrational lines with a given Δv fall into one band. For more molecules with more atoms and thus more degrees of vibrational freedom the vibrational band structure can become very complicated.

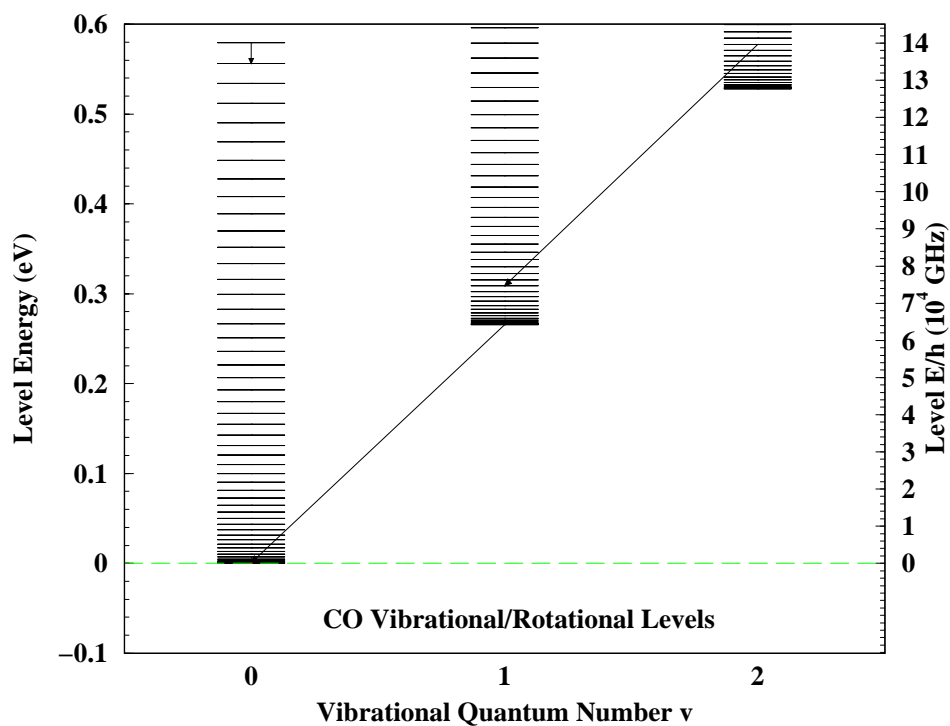


Figure 21—The energy level diagram for the lowest three vibrational levels in the CO molecule, with a few possible transitions shown. The transitions between the v levels produce molecular bands, at $4.67 \mu\text{m}$ for the two lines that are shown.

In CO the band with Δv of 1 fall near $4.67 \mu\text{m}$ and those for which Δv is 2 fall near

2.35 μm . Such bands are easily observed in the near-infrared spectra of many sources. In molecular clouds these bands are only excited when the gas is relatively hot, since the energy needed to reach them (0.25 eV or more) requires temperatures of roughly 800 to 1000 K.

Section 4: CO Observations

The CO molecule is thought to be the most common molecule aside from H_2 which will form in the ISM. Both C and O are abundant and the CO molecule is energetically favoured over such molecules as OH, CH, and other such molecules which can form from the most abundant reactive elements H, C, N, and O. Since H_2 cannot easily be observed, CO is used as the main tracer of the molecular gas in the ISM. The CO molecule has a relatively low μ value as noted above and thus is more easily collisionally excited than radiatively excited. For gas densities above 10^3 cm^{-3} the CO molecule is collisionally excited unless there is some intense source of radio or sub-mm radiation present, which will not normally be the case in the general ISM. Other molecules more often trace higher density gas in the cores of clouds.

There have been many surveys of the emission in the lower CO rotational lines, CO $1 \rightarrow 0$ at 115.271203 GHz, CO $2 \rightarrow 1$ at 230.538001 GHz, and the various isotopic molecular lines such as ^{13}CO $1 \rightarrow 0$ at 110.20137 GHz. These observations are the primary source for identification of giant molecular clouds, and for tracing the galactic rotation curve. The relatively low abundance of CO compared to H_2 or atomic H is more than offset by the higher Einstein A values for the transitions, so the CO lines can be optically thick. This is where the isotopic lines are valuable—the lower intrinsic abundance means that these lines will remain optically thin when the main lines saturate.

While the 21 cm observations of H show the broad atomic gas distribution, the CO maps show a much clumpier structure and somewhat different global structure. We are able to identify individual molecular clouds and cloud complexes over much of the galaxy, since while the CO lines are often optically thick there are different velocities for different galactic radii and so we can find clouds over a large section of the Galactic disk. In some regions the clouds complexes are confused, and we have no definitive picture of the structure in these lines of sight.

Section 4-1: The CO/ H_2 Ratio

It is normally assumed that the H_2/CO abundance ratio is constant in the ISM so a given CO column density corresponds to a definite total gas mass. In the past few years it

has become clear that this assumption is not correct, and that there are variations in the CO abundance from cloud to cloud and place to place. In general terms we expect that the CO/H₂ ratio is a function of the metallicity, but it is difficult to quantify this. There are main three ways to estimate the CO/H₂ ratio.

- 1) There is observed to be a diffuse γ -ray emission in the Galaxy. This is thought to be due to the interaction of cosmic rays with gas particles, and thus the intensity of the γ -ray emission is proportional to the H₂ column density. Assuming that the cosmic rays are not enhanced in molecular clouds, comparison of the CO emission to the diffuse γ -ray emission gives an idea of the variation in the CO/H₂ ratio. A problem for this method is the lack of strong diffuse γ -ray emission from the innermost parts of the Galaxy. Either the cosmic rays are excluded from the central regions or the CO/H₂ ratio there is higher than elsewhere in the Galaxy.
- 2) It is possible to compare dust extinction optical depths and line optical depths for lines due to minor isotopic forms of CO through various molecular clouds. Assuming a gas to dust mass ratio and the relative abundance of the isotopic forms of CO allows us to estimate the CO/H₂ ratio.
- 3) Where gas clouds are self-gravitating and in virial equilibrium there is a predicted relationship between cloud mass and its total CO emission. When the masses of clouds estimated in this way agree with other mass estimates, it indicates that the CO/H₂ ratio is not changing too much from cloud to cloud.

The standard value for the CO/H₂ ratio is expressed in terms the ratio of the CO line strength to the H₂ column density. The accepted value is $(3 \pm 1) 10^{20}$ molecules/cm²/(K km/s). There is good evidence that this ratio does not apply to all of the clouds that are observed, especially for diffuse molecular clouds observed at high galactic latitude. It seems to apply fairly well for large clouds, those with radii from 3 to 50 pc and total masses from 10⁴ to 3 10⁶ M_⊙, and for galactic radii from 2 to 8 kpc. It appears to fail in the innermost parts of the disk, in the outer parts of the galaxy, and also in low mass, gas rich galaxies such as the Magellanic Clouds. In the inner disk of M31 it appears that the standard CO/H₂ ratio is too high, and thus the clouds are more massive than estimated from the CO emission. This seems odd given that the metallicity in M31 is somewhat higher than in our Galaxy. The main conclusion from all this is that we cannot depend upon a universal CO/H₂ ratio, even scaled with the changes in metallicity.

Section 4–2: Distribution of Molecular Clouds

The cold molecular gas traced by CO has a vertical extent similar to that of OB associations, with a z range of order ± 45 to 75 pc over much of the disk. It then flares out

to a thickness of order ± 100 to 200 pc. This is attributed to hydrostatic equilibrium with the dominant force balancing the pressure being the gravitation of stars in the disk. Since the stellar surface density decreases significantly in the outer galaxy, the gas possesses a larger vertical extent out there.

There is also some evidence for very cold CO gas in the outer galaxy which may be too cold to radiate much in the rotational lines. This seems to suggest that diffuse molecular gas is the dominant component of the ISM at large galactic radii, beyond 10 to 12 kpc.

Combining the velocity information with the CO brightness temperature gives us a look at the details of the disk structure. The first such surveys were carried out in the early 1970's, and subsequent large scale surveys in the early 1980's have produced a coherent picture of how the molecular clouds are distributed in the Galaxy. The Columbia CO survey (Dame *et al.*, 1987; ApJ, **322**, 706–720) gives a good picture of the structure of the ISM in the disk. The following discussion is based upon that paper's results. In the appendix I show the velocity–galactic longitude map and the l – b map from Dame *et al.* (1987). Figure 22 shows a guide to the various features in these maps.

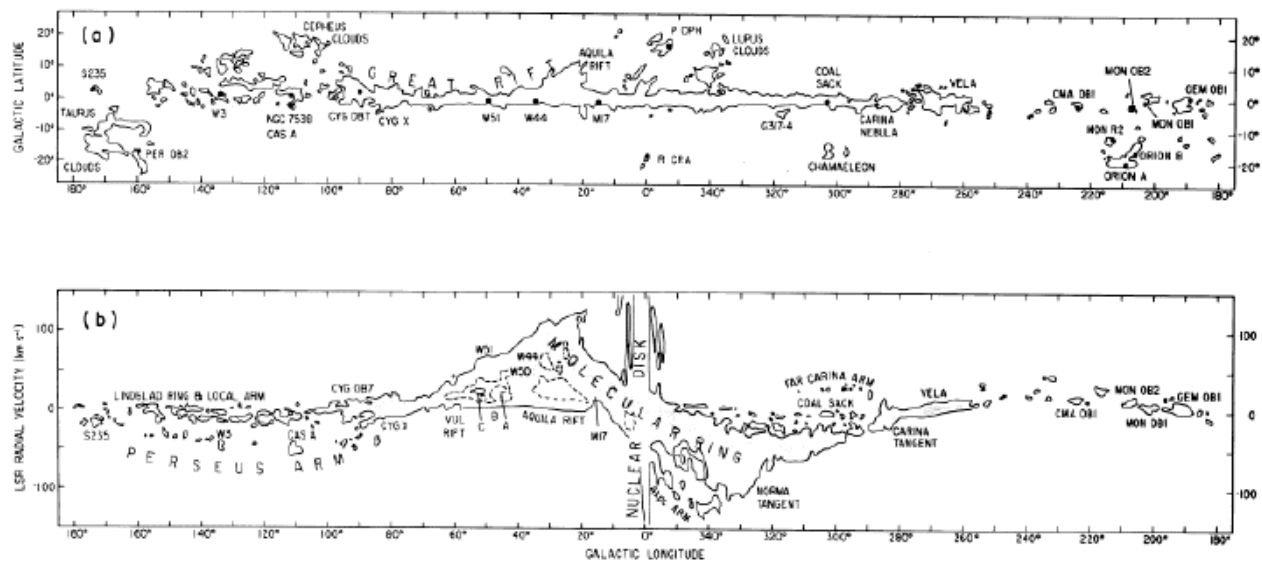


Figure 22—A schematic view of the clouds and large structures seen in the CO maps of Dame *et al.* (1987). The first panel shows features in the l – b map of total CO brightness. The second panel shows the features in the radial velocity/longitude map.

In the inner 3 kpc of the Galaxy there are only two major CO structures. In the innermost 250 pc or so there is a disk with rotational speed 220 km/s and vertical extent of about ± 100 pc. Outside this there is a ring of material between radii 500 and 750 pc, included 22° from the plane. This ring is rotating and expanding at 240 km/s. The CO

in the inner 1 kpc has a much higher surface density than anywhere outside this region.

In the early surveys the next obvious feature was an extended component covering from 3 to 8 kpc, called the *molecular ring*. These were northern hemisphere surveys, and an analogous southern hemisphere survey showed that the molecular ring is actually located at about 3.5 kpc, with spiral arms structure causing the appearance of the extended ring in the northern parts of the sky. The region from 4 to 8 kpc has about 70% of the total mass of gas, which is much different than the distribution of HI. It seems that the hole in the distribution between 1 and 3 kpc is not normal for spiral galaxies. The CO surface density seems to decrease with radius, about the same way as the stellar surface density.

Figure 23 below shows an expanded view of the Columbia CO survey results from the innermost 30° of the plane. It shows the full velocity range. The prominent line of emission to high velocities near l of 0° is the signature of the central disk. The extended emission at negative radial velocities is due to the molecular ring.

While the structure is routinely called the molecular ring, there is considerable observational support for the idea that it is actually a bar, rotated of order 25° to our line of sight to the Galactic centre. These two are not easy to distinguish from the velocity–longitude profile when random motions and the non-uniform nature of either a ring or a bar is considered. It may be that the bar only has significant amounts of molecular material at the ends, which would make a bar look very much like a ring if it is fairly wide compared to the length.

Aside from the main body of the molecular ring, there is a discrete feature in the velocity–longitude maps between 340° and 360° which is attributed to a spiral arm at about half the solar radius. Also in the fourth quadrant one sees the Carina spiral arm and some evidence of a more distant spiral arm in the same direction. Matters are somewhat confused in this region. In the first quadrant there is a prominent component coming off the molecular ring which corresponds to the “great rift” seen in optical images of the Galaxy. This is where the Sagittarius spiral arm curves out from the inner Galaxy, being a region where we look nearly along the arm and thus get extremely large amounts of extinction from the clouds there. The Carina spiral arm is thought to be the continuation of the Sagittarius Arm into the fourth quadrant.

Around longitude 90° there is a prominent region of emission that marks the OB associations in Cygnus, which seems to be a spur off of a spiral arm beyond the solar circle. This spur is called the Orion Arm, but it probably is not a real large-scale structural feature of the Galaxy.

In the outer galaxy, we observe the Perseus arm as it passes just outside the solar position. Various well known OB associations have molecular clouds associated with them

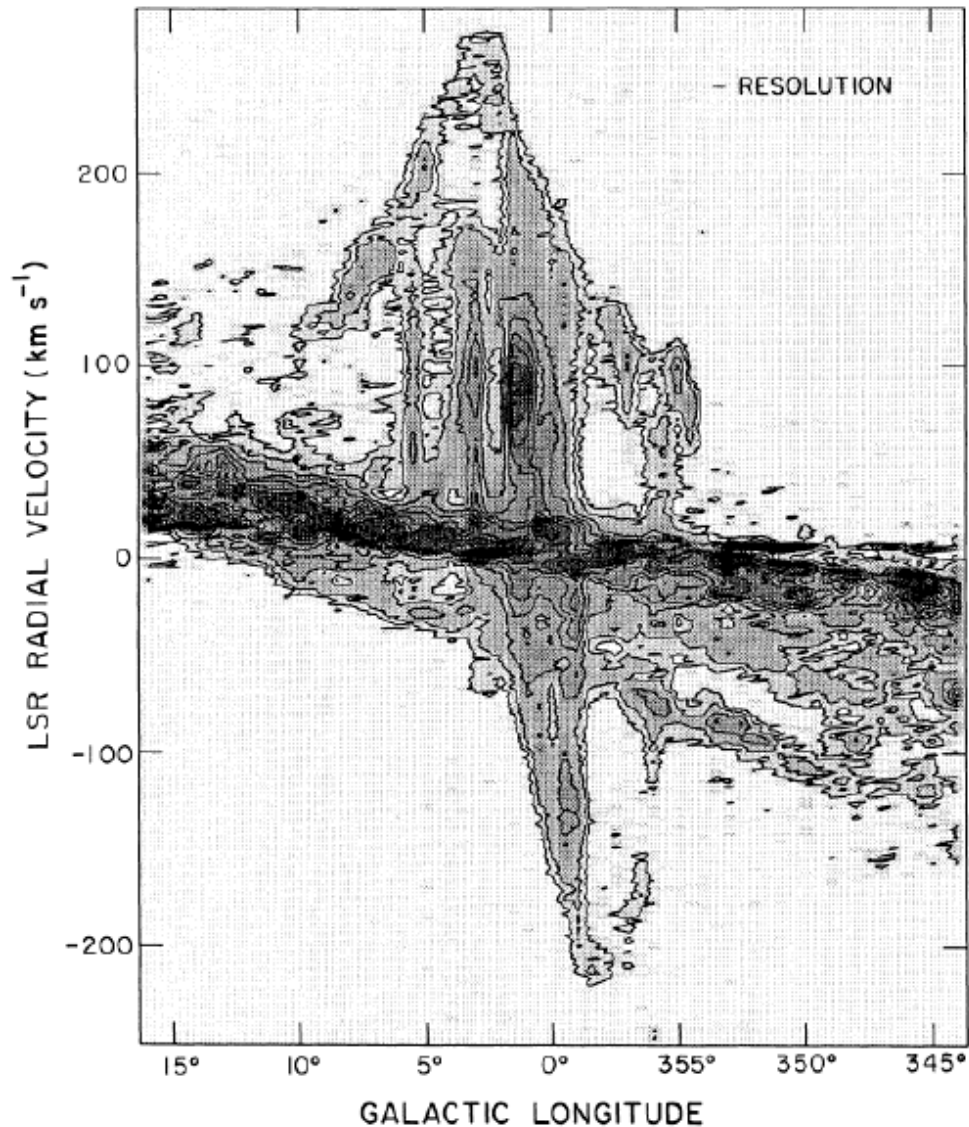


Figure 23—An expanded version of the velocity–longitude map for the innermost part of the plane, showing the molecular ring and the central disk components. From Dame *et al.* (1987).

that are easily detected in the outer Galaxy. The map does not include the Orion and Taurus molecular cloud complexes, since these nearby clouds are found significantly below the galactic plane.

It is clear that the CO does map the spiral arms, but obtaining a quantitative picture of the spiral structure has been an elusive goal. There are a number of reasons for this: the clouds have “random” velocity components of a few km/s which causes uncertainties in their kinematic distances; those distances are uncertain in the inner Galaxy since the radial velocity function is double-peaked there; finally, we do not know what the magnitude

of non-circular motions is, although in the innermost regions they are clearly of similar magnitude to the circular motion. Different groups obtain different spiral arm structure results, and none of these agrees with the optical spiral arm picture of Georgelin and Georgelin (1976; A&A, **49**, 57) which seems to be the best available approximation to the spiral structure of our Galaxy. Also the CO maps do not do a good job of distinguishing distant spiral arms. There is an outer spiral arm beyond the Perseus arm which is not clear on the CO maps. Indeed, since the "signal" of the spiral arms is much less in the outer Galaxy than in the inner Galaxy, as can be seen by comparing the CO intensity for the Perseus Arm to that for the Sagittarius-Carina Arm, the CO observations are not too useful for tracing the outer spiral arm. Similarly there are distant spiral arms beyond the Sagittarius-Carina arm, but these are not easily distinguished against the molecular ring. It is thought that there is an inner spiral arm, the Scutum-Crux arm, beyond the Sagittarius-Carina arm and possibly another arm beyond that named the Norma Arm seen in the fourth quadrant, and then possibly a "3 kpc" arm as well within the Norma Arm.

The nearby edge-on spiral galaxy NGC 891 of type Sb seems to be remarkably similar to the Galaxy in structure, and this is just as true for the CO emission as for the optical appearance. This can be seen from N. Z. Scoville, D. Thakkar, J. E. Carlstrom, & A. I. Sargent (1993; ApJ, **404**, L59). They present a velocity-position map of NGC 891 from CO 1→0 observations, which I reproduce in Figure 24. The galaxy has a CO disk near the center which is very similar to that in the Galaxy, and some type of massive molecular ring that is about twice as large in radius as the bulge of the galaxy. Estimates suggest that NGC 891 has twice the total surface density of CO gas as does the Galaxy, and about twice the CO scale height. As the mass distributions of the two systems are very similar, from their rotation curves, this means that the vertical velocity dispersion of the gas is about twice as large in NGC 891 as in our galaxy. This type of observation is important in understanding star formation, since it requires sufficient gas mass to overcome such velocity dispersions by self-gravitation.

Section 4-3: Nearby Molecular Clouds

Another result of the Dame *et al.* survey was a map of nearby molecular clouds. The picture that they arrive at is shown in Figure 25. The nearest molecular cloud is the Taurus Cloud, which is a site of intermediate mass star formation; thus the prototype pre-main-sequence star is T Tauri. There are various smaller clouds just inside the solar circle also close to us. The nearest site of active massive star formation is the Orion molecular cloud, which is somewhat further away than the Perseus OB2 cloud. The nearest fairly massive cloud complex is the Cygnus Rift/Cygnus OB7 complex.

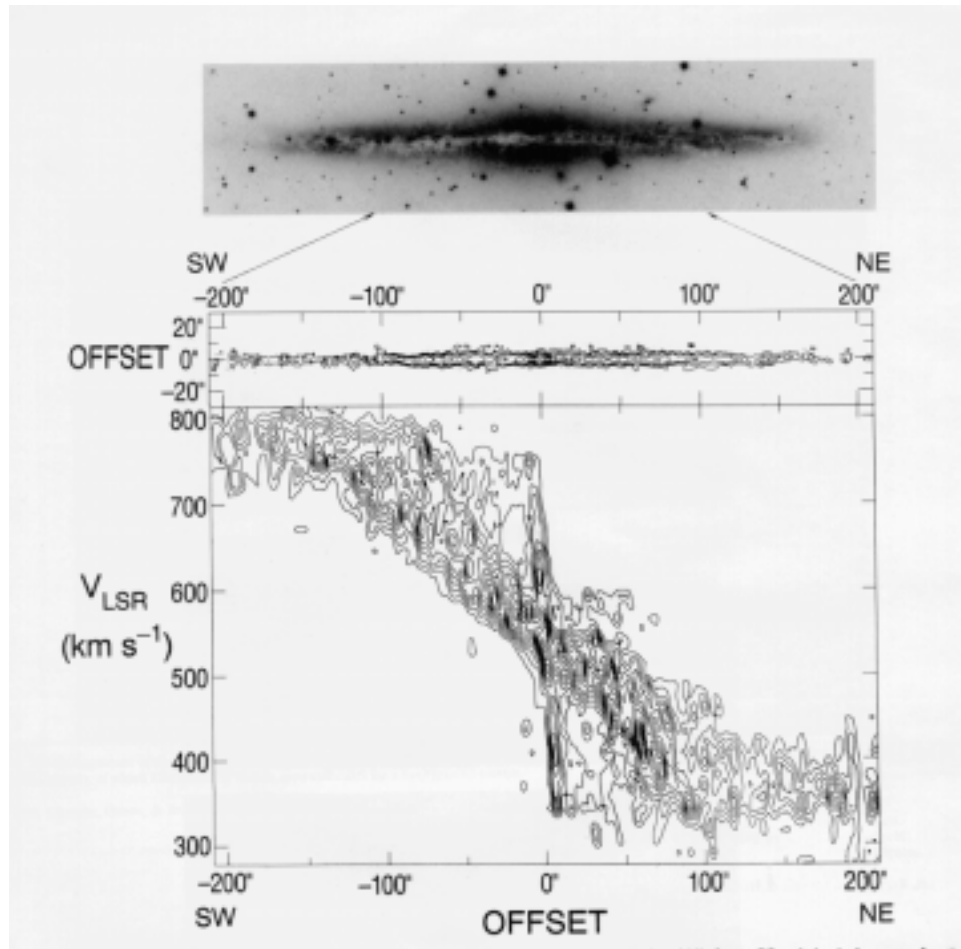


Figure 24—The intensity-position and velocity-position maps for the plane of NGC 891. The NC891 galaxy has both a molecular ring and a central disk that are remarkably similar to those of the Galaxy. This is from Scoville *et al.* (1993).

It should be noted that it is unlikely that the lines of molecular clouds just inside the solar position and just outside the solar position are due to two different molecular arms. Such a tight spacing of arms would be most unusual judging from observations of other galaxies. So as noted above the Orion Arm, which in Figure 25 includes the group of clouds beyond the Sun, is most likely just a spur off of the Perseus arm, and then the molecular clouds inside the solar position such as the Vul and Aql Rifts are part of the Sagittarius Arm. This is a major source of confusion in trying to trace the spiral arms. Indeed it is likely that spiral arms are usually not as nice and regular as is seen in a few *grand design* spiral galaxies such as M51, and that we tend to impose more order in tracing the spiral

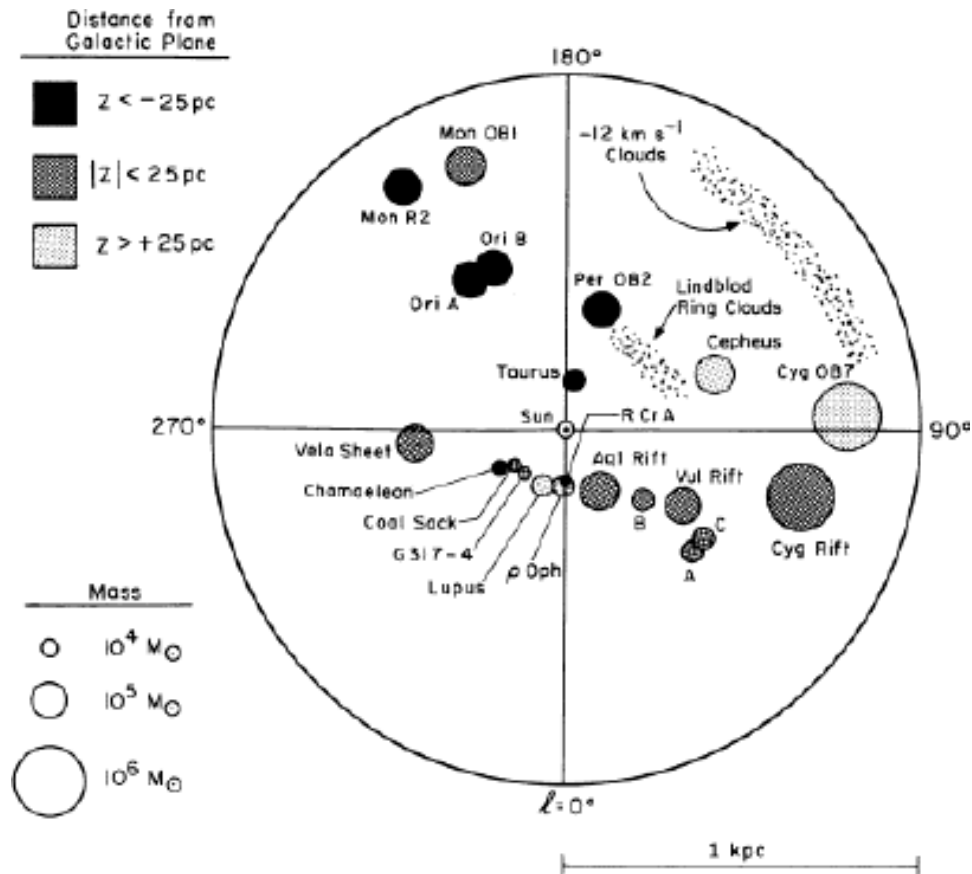


Figure 25—A map of molecular clouds within 1 kpc of the Sun from Dame *et al.* (1987). Various clouds are marked with symbols which indicate the estimated mass and the z value.

arms than really exists.

Section 5: The Canadian Galactic Plane Survey

A project is currently underway to map the northern Milky Way at high resolution in the HI 21 cm line at 1420 MHz, and also in the continuum at 408 MHz. These maps can then be compared with high resolution CO 1→0 maps recently made of the same region. Those CO observations were done with the FCRAO 14-meter radio dish. Figure 26 shows the results of the CO survey in a false-colour intensity image. This was taken from the WWW page <http://donald.phast.umass.edu/~fcrao/telescope/2quad.html>. In this part of the sky there is no ambiguity about distances from the rotation curve.

Quite a lot of structure can be seen in this image. The region around 135° galactic longitude is the W3-5 complex, which is optically visible as two regions of emission nebulosity.

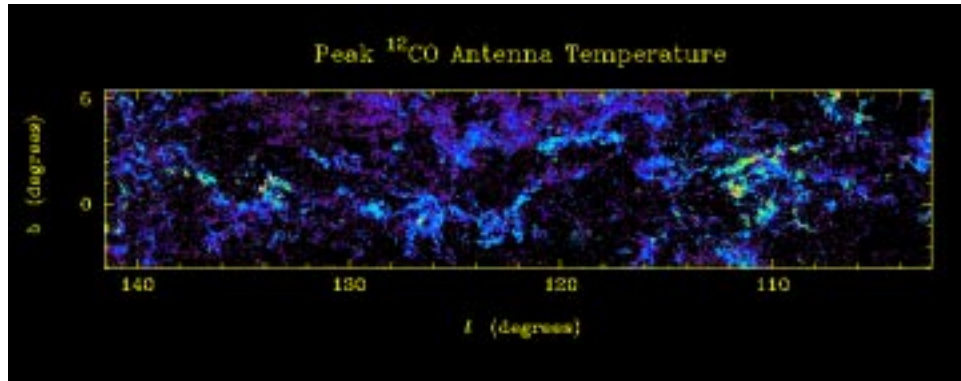


Figure 26—A CO map of the northern Milky Way in the CO 1→0 line at high resolution (50'') from the FCRAO telescope.

The 1420 MHz and 408 MHz observations are being taken at DRAO in Penticton. The group doing these observations is headed by Dr. Taylor. These maps then can be compared in detail with both the CO maps and with infrared maps made by the IRAS satellite at 12, 25, 60, and 100 μm . In Figure 27 I show some comparison of the maps at these various frequencies. Information about the CGPS can be found on the local WWW pages of the radio astronomy group: <http://www.ras.ucalgary.ca/CGPS/>.

In these images the bright regions of emission at 100 μm seen in the top panel of each page are the W3 and W5 regions, which contain hot stars and whose HII regions we can observe. The same regions show up in the dust emission due to the extra heating from the HII regions. In CO the same regions are seen to be in the Perseus arm, but there is also lots of local CO emission which has no ionized gas associated with it and which therefore is faint in the dust emission map. Looking at the 21 cm maps, the W3 and W5 complexes are associated with holes in the HI emission, and there is a lot of cold atomic gas which does not show up in CO or in dust emission. There is some tendency for the CO clouds to be inside prominent regions of HI emission, which is an indication of the need for shielding of the molecular material from the ISM radiation field. This will be discussed more later in the sections on molecular cloud properties.

When the two infrared maps are compared with the 408 MHz map of the area, it can be seen that there is a fairly close correspondence of the radio emission to the thermal dust emission. The dust is only heated to high temperatures where there is extra energy input to the ISM, and HII regions are prime examples of this. The 12 μm image shows the very hottest ISM dust emission. Compared to the 100 μm image there is more diffuse emission on the left side of the maps, so there is a large diffuse region of hotter dust grains there. This is also roughly the region of diffuse radio emission.

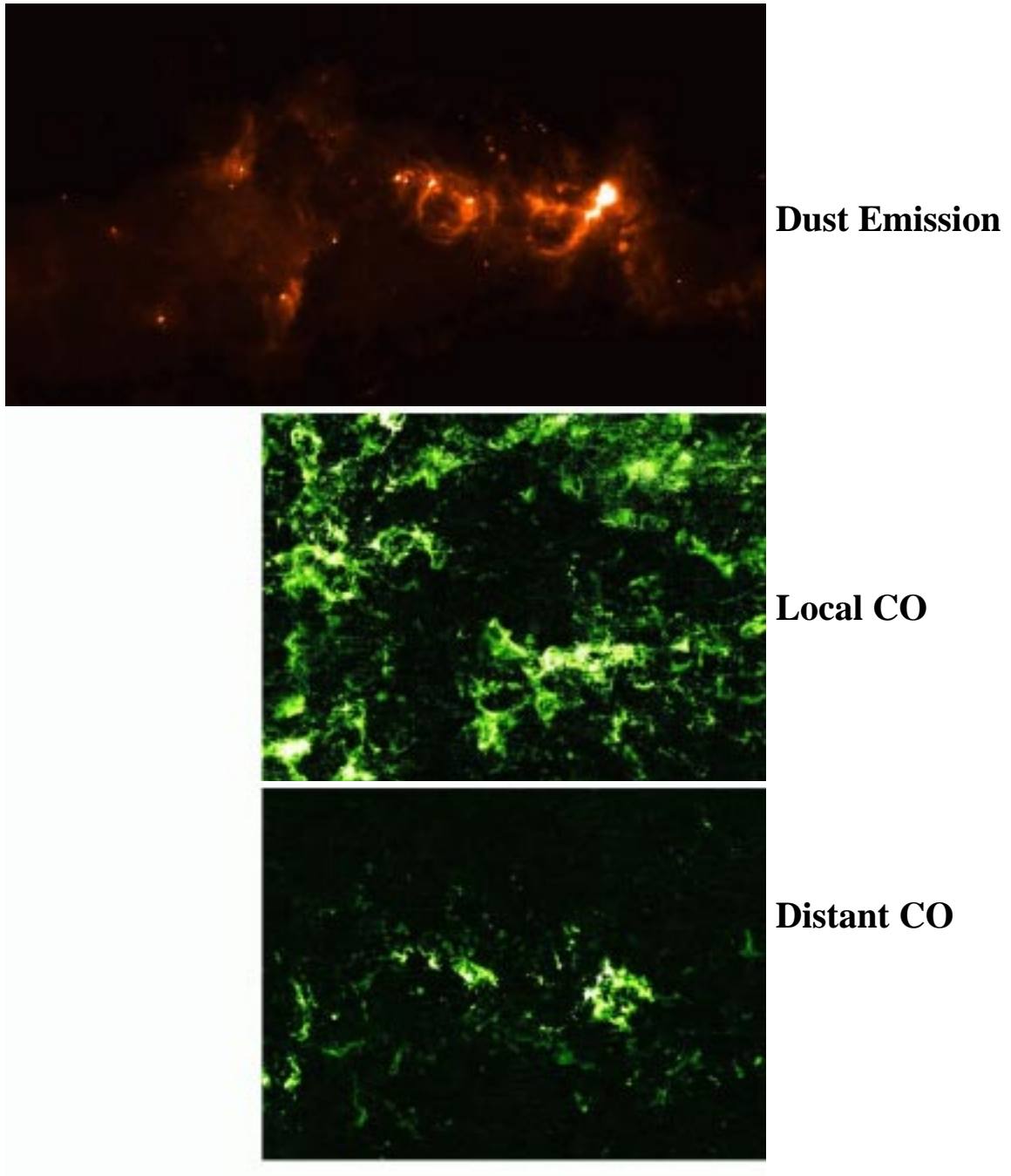


Figure 27a—Here I compare the $100\ \mu\text{m}$ image of the region near W3-5 with the CO observations from the FCRAO survey. The CO emission is divided into that from local gas and that from distant gas in the Perseus spiral arm.

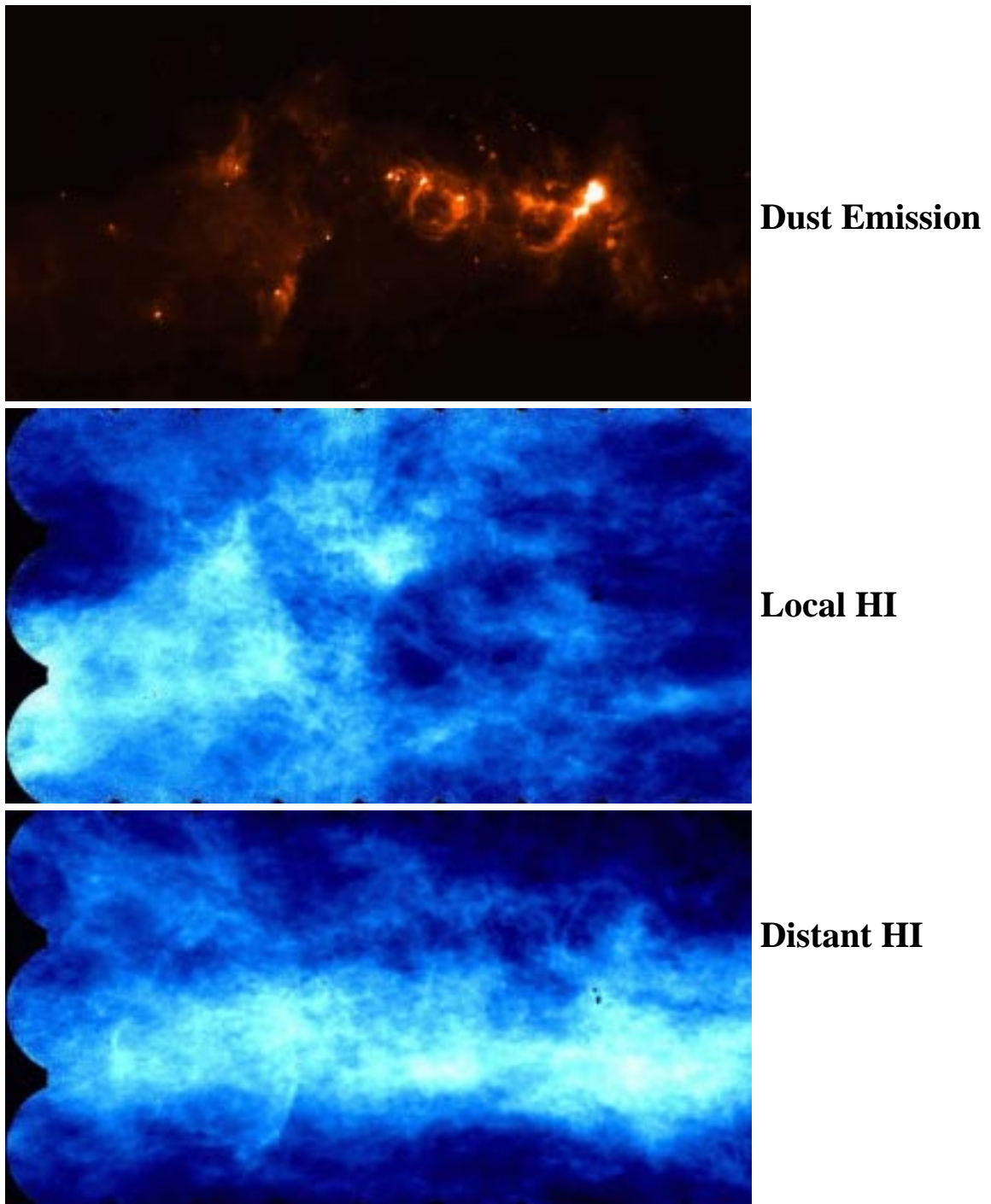
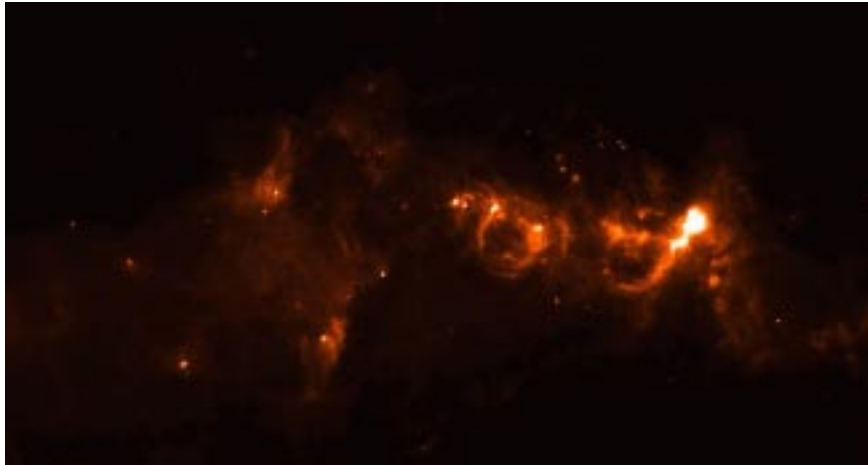
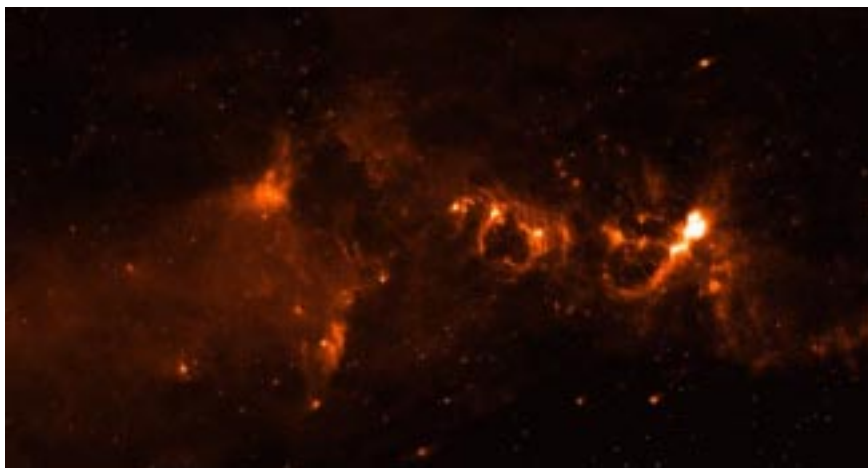


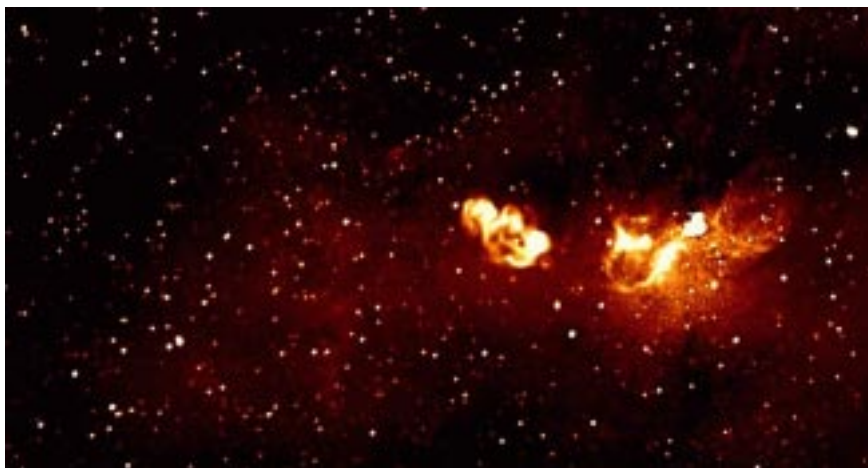
Figure 27b—Here I compare the $100\ \mu\text{m}$ image of the region near W3-5 with the 1420 MHz observations from the CGPS. The HI emission is divided into that from local gas and that from distant gas in the Perseus spiral arm.



Dust Emission
100 microns



Dust Emission
12 microns



Radio
408 MHz

Figure 27c—Finally, here is a comparison of the IRAS 100 μm map, the IRAS 12 μm map, and the CGPS 408 MHz map of the area. The 12 μm map will show small, hot dust grains. The 12 μm map shows somewhat more low level diffuse emission than is seen in the 100 μm map.

Clearly from these maps it is not simple to interpret the CO and HI observations in terms of individual clouds and cloud complexes. The W3-5 complex is certainly one structure that is present, but there are many other things seen in the CO and HI maps which are hard to understand. It is also clear from the images that the structure of the ISM clouds is rather complicated, with all sorts of filamentary structure.

Section 6: Other Molecular Lines

Of course there are many other molecular lines available for observation. The molecular lines chosen for observation are those which show us things that CO itself does not. CO is collisionally excited at relatively low gas densities and becomes optically thick when the density is high unless the region of high density is very small in extent. Thus CO maps or velocity profiles do not give us much information about the denser clouds. The CS molecule is one that is excited at higher H₂ densities, above 10⁴ per cm³, and the same is true of molecules such as HCN, NH₃, and H₂CO. The general trend is for more filamentary structure to be seen in lines of higher collisional excitation threshold.

This means that molecular clouds probably have a complex fractal-type structure, which is not surprising when the stars formed inside the clouds produce stellar winds and HII regions that compress and fragment the parent cloud. There are many clear cases of multi-generation star formation in larger molecular clouds, with plenty of opportunity for interaction.

For some nearby or simply massive clouds such as the Orion Nebula radio spectral scans are possible. For example a survey of the Orion Nebula from 208 to 262 GHz by Brake *et al.* (1987; Apj, **315**, 621) resulted in the identification of about 800 lines from molecules such as HC₃N, SO₂, SiO, CH₃OH, and OCS. In the Orion complex there are hot, dense regions with N_{H₂} of > 10⁷ cm⁻³ and *T* of about 150 K. There is a considerably different set of molecules in such hot cores than in the general cloud.

Section 6-1: Ammonia Lines

I will briefly discuss the NH₃ molecule here since the lines of this molecule are important in probing higher density and higher excitation regions of molecular clouds. Unlike CO or HCN which are linear molecules the NH₃ molecule is a symmetric top molecule with three-fold symmetry due to the three H atoms. The rotational states are denoted by the total angular momentum quantum number *J* and the angular momentum projection onto the axis of symmetry for which the quantum number *K* is used. The molecule has no electric dipole moment perpendicular to the axis, so the dipole selection rules are a little different

than in the general case where all three axes can contribute to the matrix elements of the transition. The dipole selection rules are $\Delta K = 0$, $\Delta J = 0, \pm 1$. So transitions between different K states are normally forbidden. It turns out that vibrational effects make it possible for $\Delta K = 3$ transitions to take place, but these are weak.

The main vibrational motion that is important is a change of the N atom from one side of the plane defined by the three H atoms to the other, which is called an inversion transition. Only the $K = 0$ state does not have an inversion transition due to nuclear spin statistics and symmetry requirements; all other states of given K and J are split into two closely spaced levels. The inversion transitions are allowed, and these lines in fact are the most commonly observed lines of NH_3 .

As almost all the H atoms are of the same isotope, the NH_3 molecule has overall symmetry in its wavefunction under the exchange of pairs of H atoms, leading to a splitting into ortho- and para-forms. The ortho form occurs when K is a multiple of 3 and the para form occurs for the other K values.

Levels are commonly denoted with the (J,K) values. The ground state for ortho- NH_3 is the (0,0) level. For the para- NH_3 molecule the ground state is the (1,1) level. However since it is difficult for there to be transitions from the $K = 2$ group of levels to the $K = 1$ group a large population can accumulate in the (2,2) state as well.

There are additional effects from hyperfine interactions both from electric quadrupole and magnetic interactions of the nuclear spin with the electrons. These produce line splitting of the order of 1 MHz for the quadrupole hyperfine lines and much smaller splittings for the magnetic effects. These splittings have been detected in various molecular clouds.

Figure 28 shows the energy level diagram for the lower levels of NH_3 , but without showing the hyperfine levels. The inversion doubling produces the small gaps between pairs of levels with the same K and J . Since the transitions between different K values are difficult, the levels are arranged in columns with the same K value and different J values. Each “ladder” can have transitions but crossing between the ladders is difficult. Even collisions are thought to mostly change K by 3 to preserve the overall symmetry of the molecule.

The hyperfine transitions of NH_3 are important if they can be resolved, since the relative strengths of the components are known and it is thought that there is no excitation mechanism which favours any of the hyperfine levels over others. Since the energy differences between the various components are small there is also not much of an effect due to temperature, and so from the observed line strengths we can derive the optical depths of all the lines directly. This avoids the problems that can occur in using isotopic lines such as variations in excitation and in isotopic ratios.

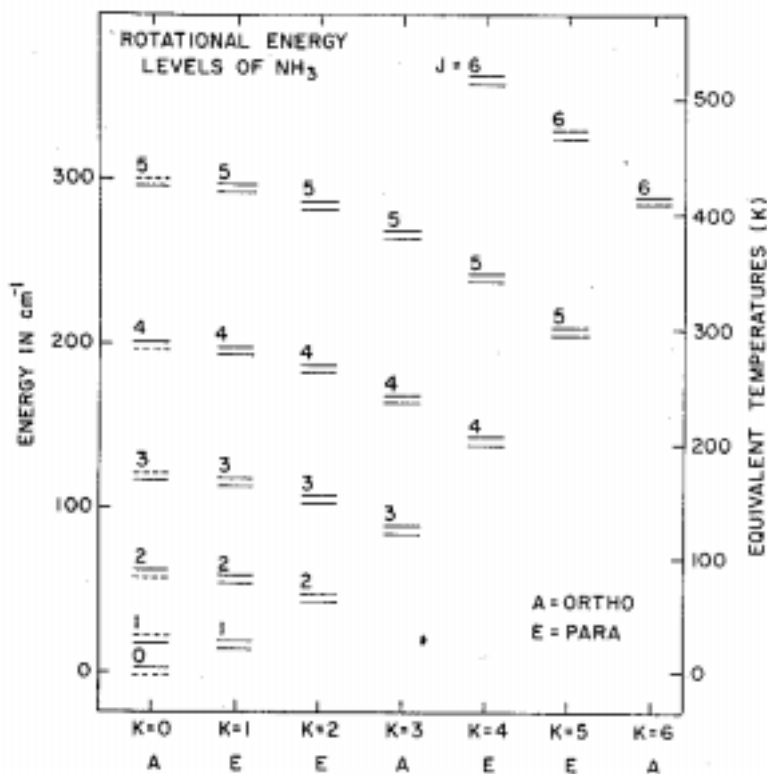


Figure 28—The energy level diagram for the lower rotational levels of NH₃. Levels are marked by the J and K quantum numbers, and arranged in columns of constant K since the dipole transitions require $\Delta K = 0$. When $K = 0$ the inversion doubling does not occur hence the excluded levels are shown via dashed lines.

The inversion transitions of NH₃ can be excited at a rather low temperature as seen in Figure 28 above. The (1,1) and (2,2) inversion lines are most often observed since these are the transitions at the very bottom of the ladders for para-ammonia.

The other interesting property of NH₃ for molecular cloud observations is that it has transitions with a wide range of A_{ul} values. Since the populations are determined by the competition between collisional excitation by H₂ (mostly) and the radiative decay rate, having a wide range of A_{ul} values means that NH₃ produces useful lines at a wide range of densities. The inversion transitions have higher A_{ul} values than most of the ladder transitions. So the inversion transitions in the lowest states for each K are excited at low temperatures and densities, while the inversion transitions from the higher states in any given K -ladder require high densities to excite and are therefore probes of high density gas (N_{H_2} from 10^8 to 10^9 per cm³). Also just which of the lowest K levels are excited tells us something about the temperature and density in a given cloud.

The inversion lines have frequencies from 21 to 25 GHz for most of the lower rotational levels. The transitions between the states are at much higher frequency and can only be observed in the sub-millimeter and far-infrared. However we do not really need to observe these transitions when we can observe several inversion transitions. The (1,1) and (3,3) lines at 23.6945 and 23.8701 GHz are often used since they probe colder and warmer regions of a cloud (the energies above ground are equivalent to T values of 23.4 and 124.5 K). In warmer regions the (6,6) inversion line also shows up.

Section 7: Molecular Masers

The first radio molecular line ever detected was a strong line at 1612 MHz, soon followed by associated lines at 1665, 1667, and 1720 MHz. The transition frequencies matched transitions expected from the OH molecule but the line intensities were much different than expected. In thermodynamic equilibrium if the emission is optically thin then the expected line ratios depend upon the corresponding $g_u B_{ul}$ values and come out to about 1:5:9:1 for the four lines. If the emission is optically thick at a reasonable (kinetic) temperature, such that the line frequency is much less than kT , all four lines should have nearly the same strength. The temperature has to be larger than $h\nu/k$ for the latter approximation to hold, but for these lines that is easy to satisfy since $h\nu/k$ is less than 0.1 K.

Instead the four lines show a range of odd behaviors in different environments. In circumstellar shells caused by mass loss from M-type stars the 1612 MHz line is usually much stronger than the other lines. In ISM clouds the main lines (1665/1667 GHz) behave more or less as expected in many cases, showing up in absorption, but the satellite lines (1612/1720 MHz) usually have odd properties such as one being in emission and the other being in absorption. The line in emission has a very high or negative excitation temperature. In other sources, particularly near HII regions or areas of active star formation, the main lines are in emission. It appears that these lines are produced right at the interface of an HII region and a molecular cloud.

The transitions in OH which are subject to maser emission are all sub-levels of the ground rotational state of OH. The orbital angular momentum quantum number L is 1. The rotational angular momentum quantum number takes values 0, 1, 2, and so on. I will call this value R here. Interaction with the spin of the unpaired electron in the molecule produces J values for the angular momentum excluding nuclear spin effects of either $L + R + 1/2$ or $L + R - 1/2$. These form two sets of rotational levels. The transitions that invert the spin-orbit coupling, changing the J quantum number for the same R , can occur but are weaker than transitions which leave the spin-orbit coupling unaltered. (Such

transitions are forbidden when simple spin-orbit coupling applies, but the situation for OH is more complex so these transitions can occur.) The lowest rotational state has J of $3/2$.

Interaction with the nuclear spin produces total angular momentum quantum number values F of either 2 or 1 for the ground state. There is also a small interaction with the other electrons in the molecule which produces Λ -doubling of the levels—the states of even or of odd parity have slightly different energies. Thus between the two processes four levels are present within the ground state. Normal transitions require ΔF to be ± 1 or 0 but with $0 \rightarrow 0$ forbidden. The 1665 and 1667 MHz lines have ΔF of 0 while the other two lines have ΔF of ± 1 . Figure 29 shows the energy level diagram for the lowest few rotational states.

In Figure 29 the transitions within the rotational levels and between the first excited rotational level and the ground rotational level are marked. All of these are permitted transitions. As can be seen, there are more transitions into the $F = 2$ states than into the $F = 1$ states.

Transitions have the selection rules ΔJ equal to 0 or ± 1 , ΔF equal to 0 or ± 1 , and must preserve parity. Looking at the first excited state of the molecule, the F values of 3 or 2 are not the same as those of the ground state. What happens is that all four of the excited state levels can have transitions to the $F = 2$ pair of ground state levels, but only two of them can have transitions to the $F = 1$ pair of ground state levels. If I ignore statistical weights and assume that all transition rates are exactly the same, then the $F = 2$ ground state levels will receive twice as many incoming electrons as the $F = 1$ pair. A similar result, although in the opposite sense, occurs in transitions from the next excited state. There is no such effect in transitions down from the next highest state, but it happens again for the fourth excited state.

As the energy separations between the sub-levels of the ground state are very small, the equilibrium level populations of these are 1:1 once the statistical weight effects ($2F + 1$) are taken out. Thus, any process that delivers electrons to one pair of levels but not the other pair will tend to cause a population inversion in one of the satellite lines while it does not effect the main lines.

Thus in the OH molecule the maser population inversion occurs when there is some mechanism to produce transitions to the excited rotational states, and when the electrons come back down to the ground state they will tend to produce a population inversion. This can be the case, for example, if the transition from the first excited state to the ground state is optically thick and there are no collisions to change the populations of the ground state sub-levels, so with many transitions up and back down due to the line transitions with a wavelength near $120 \mu\text{m}$ in the rotational line a significant population inversion can

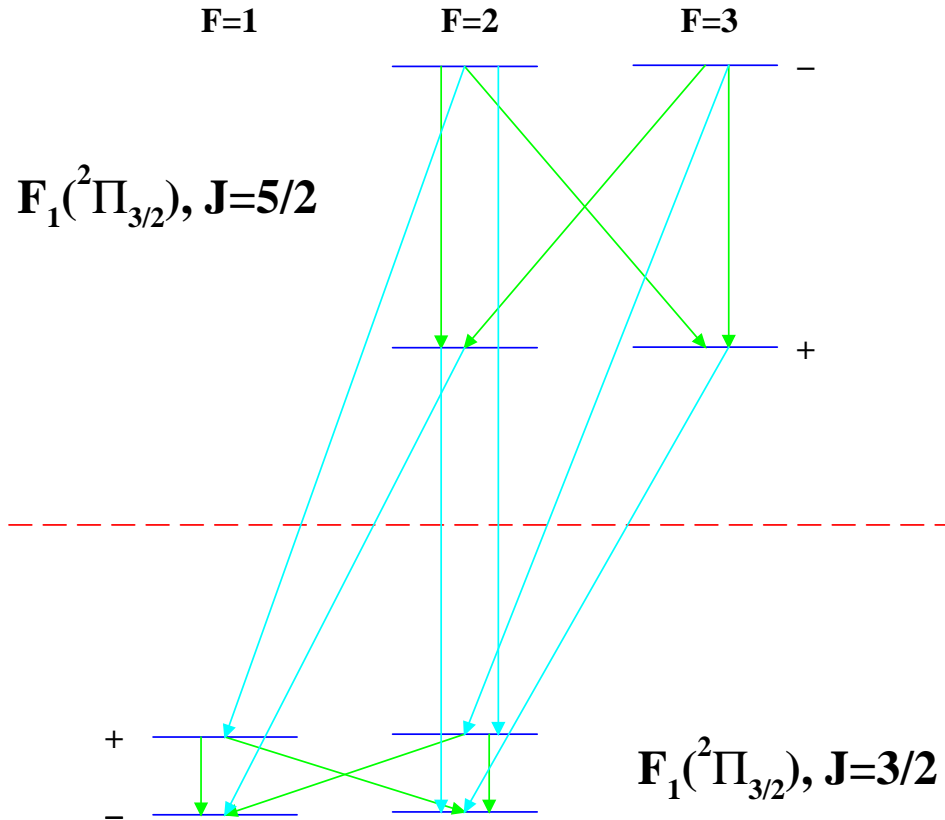


Figure 29—The energy level diagram for the 8 lowest rotational levels in the OH molecule. Levels are distinguished by the J and F quantum numbers along with the parity (+ or -). The transitions in the ground state sub-levels produce maser transitions. The dotted line across the center of the plot indicates that the energy values are not to scale—the energy gap between the $J = 5/2$ and $J = 3/2$ levels is 400 times larger than the energy differences in between the levels of the $J = 5/2$ state. Transitions are marked. All of these are permitted electric dipole transitions; those with $\Delta J = 1$ have wavelengths close to $119.3 \mu\text{m}$. The transitions between the sublevels for the ground state occur near 1.67 GHz and those for the first excited rotational state occur near 6.02 GHz.

result. Under normal laboratory conditions the transitions between the sub-levels occur via collisions and such an inversion does not occur.

It is also possible to have collisional pumping of the upper rotational levels if that type of collisional transition can occur much more efficiently than transitions between the various sub-levels.

With the two excited states tending to produce opposite types of inversions, detailed calculations need to be carried out to predict what happens when both of these levels are populated. It turns out that the 1612 MHz maser is favoured over the 1720 MHz maser

due to statistical weight effects. Simply put, the 3 levels with $F = 1$ and even parity are more easily overpopulated than the 5 levels with $F = 2$ and even parity. To make a 1720 MHz maser the cascades down from the second excited state have to be suppressed compared to the cascades from the first excited state. Either the temperature has to be low and only collisional pumping is occurring, or the transition across the rotational ladders has to be weak compared to that within the rotational ladders. The second situation can occur when the optical depth in the cross-ladder lines is small and that in the inter-ladder transitions is larger than 1, which only happens for relatively small OH column densities as it turns out. The first situation requires gas kinetic temperatures of less than 200 K. When radiative transitions provide the pumping or when the kinetic temperature is higher the 1612 MHz line is always the maser line.

It turns out that the 1720 MHz line is only seen in maser emission under unusual circumstances whereas the 1612 MHz maser line is quite common, which argues for radiative pumping of the line.

The OH main lines are usually thermal in origin in the ISM or in circumstellar envelopes. However they are seen in maser emission in HII regions and in some stars with circumstellar dust shells. In the latter case the cause of the pumping is still radiative, and is due to the slight frequency shifts in the transitions of different parity. If the exciting source has a rising infrared spectrum there is a slight preference for transitions to the higher sub-level, and since the transitions back down in the main rotational ladder do not change the parity or select either F value this leads to slight population inversions in the main line upper levels. This can only take place when only radiative transitions are important, since collisional effects would tend to erase any population inversion. The pumping is only effective when the radiation field of the exciting source has a steep slope in the infrared.

In HII regions the main-line maser emission is much stronger than in late-type star circumstellar shells, and here the source of the pumping is not understood. The masers occur at the edge of the ionized zone, and while there is observed to be intense infrared radiation in such regions due to a combination of shock and radiative heating of the dust by the HII region it is still hard to see how the very strong masers can be produced. Estimates of the pumping efficiency seem to show that it cannot be due to radiative pumping simply because the dust is mostly too cold to selectively pump one set of transitions over the other. On the other hand if collisional pumping is producing the inversion then we do not understand how this happens, since when collisions are frequent deviations from thermodynamic equilibrium tend to be reduced not enhanced. The strength of the masers would require a high rate of collisions to feed in the required energy, and it is then hard to find

a way to select one set of levels over the other.

Section 7-1: Other Maser Lines: H₂O

There are many other maser lines which have been observed. The mechanisms involved vary from molecule to molecule. The second masing molecule discovered was H₂O. The rotational transitions of H₂O are complicated because the molecule is not a linear one, and the two hydrogen atoms are quite mobile. The molecule has ortho- and para- forms since the two hydrogen atoms are symmetrically placed with respect to the molecular symmetry axis, and the ortho- form of water is the source of the observed transitions.

The rotational levels of H₂O are labeled by the total (rotational) angular momentum quantum number J and by the quantum numbers for the projections K_- and K_+ onto the two axes of the molecule. (The molecule is planar so the third dimension is not important.) In the ortho-water molecule J values must be larger than zero and the difference $K_+ - K_-$ must be odd; also J must be \geq the K values. The lowest energy rotational level for a given J value is that where K_+ is the largest. It turns out that the lowest energy J levels have much larger transition strengths and collisional cross-sections than do the other lines with different K_+ values. Most of the molecules are in these levels. Population inversions occur between these so-called *backbone* levels and levels that are not part of the backbone, which are not very efficiently populated. Some of the observed water maser transitions are forbidden transitions, while others are normal permitted transitions. Due to absorption by water in the Earth's atmosphere, water masers can only be detected if the line is very strong and the atmospheric absorption is relatively weak: this means that thermal water lines have not been observed, and maser lines have most often been observed from higher rotational states which require temperatures of more than 400 K to excite.

The first water maser line detected was the $6_{16} \rightarrow 5_{23}$ transition at 22.23508 GHz. When the line was first detected its in various star-forming region the brightness temperature ranged up to 60 K with a relatively large beam size. Subsequent interferometry measurements have shown that individual maser spots have brightness temperatures in excess of 10^{14} K in the W49 molecular cloud complex, which certainly requires a non-thermal origin for the emission. Most of the water maser observations have been carried out at this wavelength, because it is the lowest frequency rotational line of water from the lowest vibrational state. The other lines are generally found in the sub-mm or far-infrared wavelength ranges, where observational sensitivity is normally less and where atmospheric absorption is larger than at 22 GHz. About 25 years separated the discovery of the 22 GHz water maser and the firm detection of other water maser lines, such as the para-H₂O 183 GHz $3_{13} \rightarrow 2_{20}$ line and 325 GHz $5_{15} \rightarrow 4_{22}$ line, and the ortho-H₂O 10₂₉ \rightarrow 9₃₆ line

at 321 GHz. A maser line at 658 GHz from a rotational transition in a higher vibrational level has also been detected in some circumstellar shells, but that line does not occur in molecular clouds.

The levels where the maser emission originates require a high kinetic temperature for collisional excitation. In circumstellar shells the H₂O masers occur only in sources with higher mass-loss rates, and the H₂O masers occur in a region of smaller radius than does the OH maser emission. In such cases the gas is at a high enough temperature for direct thermal excitation of the levels that produce the masers, although the maser from the higher vibrational state is more difficult to explain in this regard since the required excitation energy is rather large.

In molecular clouds the H₂O masers are seen where star formation is taking place, and the masers are now taken to be a direct sign of star formation. The water masers occur outside any HII regions and away from where the OH masers occur in such clouds. The most luminous H₂O maser source in the Galaxy is W49N, where it is estimated that the maser luminosity is 1 L_☉. The maser emission is complex, usually showing multiple components at different velocities which vary with time. When the emission is mapped it is found that it is composed of many small regions of maser emission which have a complex structure in both spatial and kinematic terms. It is found that maser peaks with small radial velocities with respect to the molecular cloud have large proper motions and are brighter, and those with large radial velocities with respect to the molecular cloud have small proper motions and are weaker in intensity. It therefore is likely that the space velocities of both groups of masers is the same and that the radiation is beamed perpendicular to the direction of motion.

Studies of various of these maser regions suggest that there is both turbulent motion and the large-scale motion of the gas, and that the maser spots form and disperse over periods of a decade or so as these motions produce short-lived higher density regions where the maser gain is increased enough to produce strong emission. The maser profiles are constantly changing in velocity and intensity distribution. The current theory is that strong stellar winds from young stars produce the large-scale motions and the turbulence in the surrounding gas, and that the masers are powered by shock excitation of the gas. Such shocks are the easiest way to excite the molecules to relatively high rotational levels.

Section 7-2: Rare Maser Lines

A completely different type of maser emission is seen in SiO, where many maser lines have been detected. Like CO, SiO is a simple linear molecule with a straight-forward energy level diagram. The maser lines are observed in the rotational transitions of higher

vibrational states, with 6 or more consecutive rotational lines all showing maser emission in some of the vibrational states. There is also sometimes maser emission in lines from the ground vibrational state.

Maser emission from SiO is common in late-type stars, where they are thought to actually come from the outer atmosphere of the star, but is relatively rare in star formation regions even though the lines were first discovered in the Orion Nebula. SiO masers are produced when the molecule can be excited into the higher vibrational states, which requires kinetic temperatures of the order of 1500 K or radiation in the near-infrared. Population inversions occur because transitions which change the vibrational and rotational state together are much stronger than the pure rotation transitions: thus when the various ro-vibrational lines are optically thick (and so de-excitation of the higher ro-vibrational levels is inefficient because the radiation cannot escape) the higher J levels get overpopulated just because there are more ways to excite these levels compared to those of low J . As long as there is lots of radiation or collisions to excite the levels, and this excitation does not change much with J between the vibrational levels, and the ro-vibrational lines are optically thick this means that all the excited vibrational state J levels are likely to have a population inversion. The pure rotational transitions are rare, but when they do occur maser emission results for all these lines.

It turns out that SiO masers are fairly easy to understand for the atmospheres of late-type stars, but are difficult to explain for molecular clouds or star formation regions. For some years the Orion Cloud was the only such cloud where the masers were seen, until observations with the 45-m Nobeyama radio telescope discovered other such masers in W51 and Sgr A. These SiO masers are quite unlike that from Orion or each other. The only conclusion that can be drawn at this point is that SiO maser excitation conditions are difficult to produce in molecular clouds, as compared to late-type star circumstellar shells. The SiO masers in late-type stars are thought to be collisionally excited, although it is still possible that they are excited by the strong infrared radiation of the star. In Orion the maser is also thought to be collisionally pumped, and is associated with an extremely energetic stellar wind outflow from a very young OB-type protostar (near source IRc2, but not clearly identified due to high levels of dust extinction in the vicinity) with a fairly high luminosity. It may be that exceptionally strong shock excitation is needed to produce SiO masers in molecular clouds.

There are various other species where maser emission has been seen in star formation regions, although they have not been as widely observed as OH or H₂O. These include NH₃, CH₃OH, and H₂CO. In some cases the lines are just more difficult to observe than those of OH or H₂O and in other cases the lines are not strong masers. For all these

molecules the pumping mechanism is difficult to determine. Being unable to get detailed physics from analysis of the lines without some understanding of the pumping process, these lines do not yet give us any information beyond that which the OH and H₂O masers provide.

Section 8: Megamasers

Starting in the 1970's, maser emission was detected in external galaxies. Originally OH maser emission was discovered in the irregular galaxy M82 and in NGC 253. The maser emission was some 10 to 100 times as luminous as the most luminous OH maser sources in our Galaxy, and in both cases it was suggested that the maser was amplifying emission from a background source. Later in the 1980's far stronger maser sources were discovered, with total luminosities ranging up to 10^8 times that of the most luminous OH maser sources in our Galaxy. These were called *megamaser* sources; the prototype is Arp 220, which seems to be a case of two galaxies undergoing a collision with accompanying strong star formation. The megamaser sources tend to have very strong infrared emission at longer wavelengths, which is due to dust of temperature around 60 K. The infrared emission and the maser emission come from a highly obscured region of the galaxy. The OH masers are seen in the 1665/1667 MHz main lines, and the emission is so wide that the two lines overlap. The line profile can be fit by assuming that there is a disk of material rotating at about 125 km/s which is producing the OH maser emission. What we see appears to be maser amplification of a background radio continuum source—presumably the nucleus of the galaxy—by a large group of molecular clouds. The population inversion is produced by the strong infrared radiation, but is only modest in magnitude. The reason for the large total luminosity is that there is a large amount of gas around the nucleus all of which is producing maser emission at a low efficiency.

Another class of extragalactic megamaser has been detected in the H₂O 22.235 GHz line. These masers are of relatively high luminosity compared to the more luminous galactic sources such as W51N, and similar H₂O maser sources observed in galaxies in the Local Group, and the maser is situated in a small volume right in the galactic nucleus. These masers are seen in galaxies which may have nuclear activity, such as the Seyfert galaxy NGC 1068. The maser emission seems to occur in a disk of relatively small radius (a few pc) right at the dynamical center of the galaxy. In a number of cases observations of such disks have been used to infer that there is a massive, compact object at the center of the galaxy. It may be that the maser is excited by either radiation or shocks associated with this compact object, but it has also been suggested that the excitation mechanism is the

same as for star formation regions in the Galaxy and that the larger luminosity is just a result of a burst of star formation in the nucleus. Some support for this idea comes from the observation that the maser strength is not well correlated with the strength of the AGN-type activity in the nucleus.

Appendix: The Dame *et al.* (1987) global CO maps of the Galaxy

Here I reproduce the CO maps from Dame *et al.* (1987) in six panels. Each shows only a portion of the map since the original is a fold-out which is much larger than a standard page.

The first three pages show the brightness temperature map assembled from the full set of Columbia data. In these plots the x and y axes are galactic longitude and latitude in degrees, and the plot shows contours of the observed antenna temperature. This shows various clouds and features for which a schematic is given in Figure 24.

The second three pages show the velocity-position map, similar to Figure 25 where the inner portion is shown in detail. Here the y axis is the LSR radial velocity in km/s. Again, a guide to the structures that are seen is given in Figure 24. Only the region within $\pm 3.5^\circ$ of the plane is used in making this map, hence the Orion and Taurus clouds are not seen here.

